Detection of Short-scale Turbulence in the Next Generation of Tokamak Burning Plasma Experiments
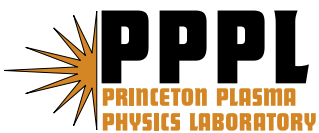
E. Mazzucato

Revised November 2006

PPPL
PRINCETON PLASMA PHYSICS LABORATORY

Princeton Plasma Physics Laboratory
Report Disclaimers

PPPL Report Availability

Princeton Plasma Physics Laboratory:

http://www.pppl.gov/pub_report/

Office of Scientific and Technical Information (OSTI):

http://www.osti.gov/bridge

U.S. Department of Energy:

U.S. Department of Energy
Office of Scientific and Technical Information
P.O. Box 62
Oak Ridge, TN 37831-0062
Telephone: (865) 576-8401
Fax: (865) 576-5728
E-mail: reports@adonis.osti.gov

Detection of short-scale turbulence in the next generation of tokamak burning plasma experiments

E. Mazzucato[1]

Princeton Plasma Physics Laboratory, Princeton, New Jersey 08543, USA

ABSTRACT

In this paper, we discuss the use of coherent scattering of CO_2 lasers for high resolution measurements of short-scale turbulent fluctuations in the next generation of tokamak burning plasma experiments. The unique feature of the proposed scheme is the oblique propagation of the probing beam with respect to the magnetic field, with the toroidal curvature of field lines playing a major role in improving the spatial resolution of measured signals. In addition, small scattering angles and negligible wave refraction effects minimize the size of needed ports – a matter of vital importance for a plasma diagnostic that must operate in the hostile environment of a burning plasma.

---

[1] Electronic mail: mazzucato@pppl.gov

1. Introduction

The direct impact of plasma confinement on the feasibility of an economical fusion reactor makes the investigation of plasma transport one of the most important tasks for the next generation of DT burning plasma experiments – such as IGNITOR and ITER [1,2] – where for the first time the kinetic energy of charged fusion products will be the dominant source of plasma heating. Consequently, since both theory and experiments suggest that plasma transport in tokamaks exceeds neoclassical values because of the existence of a short-scale turbulence [3,4], the study of the latter will be of paramount importance for these experiments.

The main difficulty in choosing a method for the measurement of turbulent fluctuations is the scarcity and limitations of available diagnostics. For example, the method of coherent wave scattering, that was so prominent in early fluctuation studies [5-9], has a poor spatial resolution – very often larger than the plasma minor radius. The method of Beam Emission Spectroscopy [10] is sensitive only to relatively large-scale fluctuations, and the negative ion beams required for accessing the main core of a burning plasma are still under development. Likewise, microwave reflectometry can detect only large-scale fluctuations, and the interpretation of signals from the outer plasma region - where turbulent fluctuations are very large - is extremely difficult [11,12].

Meeting the requirements of plasma diagnostics will be extremely difficult in the next generation of burning plasma experiments, where plasma accessibility will require penetration of not only toroidal magnets and vacuum vessels, as in present experiments, but also of thick insulating layers and radiation shields. Inevitably, only the most simple and reliable diagnostics will survive in such a hostile environment.

Ideally, what is needed is a method capable of detecting all types of short-scale turbulent fluctuations without the need for large ports. This is a daunting task given the

2

variety of fluctuations in tokamak plasmas – from the Ion Temperature Gradient Mode (ITG) and the Trapped Electron Mode (TEM), both with the scale of the ion Larmor radius, to the Electron Temperature Gradient (ETG) mode with the scale of the electron Larmor radius [3,4]. As an example, in ITER [2] with an average plasma temperature of 10 keV and a magnetic field of 5.3 T, the wave number of possible fluctuations varies from 1-2 cm^{-1} for the ITG/TEM modes, to 50-100 cm^{-1} for the ETG mode. In IGNITOR [1], because of its high magnetic field (13 T), we expect shorter fluctuations by a factor of ~2.5.

In this paper, we discuss the possibility of employing coherent scattering of CO_2 lasers for localized measurements of turbulent fluctuations in a tokamak burning plasma experiment. This is motivated by some important advantages of this technique, such as the availability of high power single-mode lasers, negligible wave refraction effects, and relatively modest requirements for the size of needed ports.

2. Coherent Scattering of Electromagnetic Waves

Coherent scattering of electromagnetic waves is a powerful technique, capable of providing the spectral power of turbulent density fluctuations. It was employed extensively in early studies of plasma turbulence, including the first detection of short-scale turbulence in tokamaks [5,6].

The process of coherent scattering of electromagnetic waves by turbulent density fluctuations can be characterized by the differential cross section

$$\sigma = (e^2/mc^2)^2 S(k,\omega), \tag{1}$$

where $S(k, \omega)$ is the spectral density of plasma density fluctuations [13]. The frequency (ω) and wave vector (k) of fluctuations must satisfy the energy and momentum conservation, i.e., $\omega = \omega_s - \omega_0$ and $k = k_s - k_0$, where superscripts s and 0 refer to

scattered and incident waves, respectively. Since for the topic of this paper $\omega_s \approx \omega_0$ and $k_s \approx k_0$, the scattering angle θ must satisfy the Bragg condition

$$k = 2k_0 \sin(\theta/2). \tag{2}$$

The instrumental resolution of scattering measurements is limited by the size of probing and scattered beams, that in this paper we will assume having a Gaussian amplitude profile $A(r_\perp) = \exp(-r_\perp^2/w^2)$, with $r_\perp$ a radial coordinate perpendicular to the direction of propagation and w the beam radius. The wave number resolution of measured fluctuations, then, depends on the beam spectrum $G(\kappa_\perp) = \exp(-\kappa_\perp^2/\Delta^2)$, where $\Delta = 2/w$ and $\kappa_\perp$ is the wave number component perpendicular to the direction of propagation. For example, we get $\Delta \approx 0.7$ cm^{-1} for w=3 cm, which is satisfactory when compared to the wave number of expected fluctuations. However, if we take the size of the common region between the probing and the scattered beam as a measure of spatial resolution (δl), we get $\delta l \approx 2k_0 w/k$, from which one might conclude that it is difficult to perform localized measurements of plasma turbulence with coherent scattering of electromagnetic waves. Fortunately, this estimate is valid only for an isotropic turbulence, which is not the case in tokamak plasmas where short-scale fluctuations satisfy the relation $\mathbf{k} \cdot \mathbf{B}/B \approx 1/qR$ [3,4] (with q the magnetic safety factor and R the plasma major radius). For all practical purposes, this can be written as

$$\mathbf{k} \cdot \mathbf{B} = 0. \tag{3}$$

In this paper, we will impose this constrain to the range of possible fluctuations, i.e., we will assume the wave vector of plasma fluctuations to be perpendicular to the magnetic field. In this case, then, the spatial variation of the magnetic field direction can modify the instrumental selectivity function by detuning the scattering receiver [9,14]. This can be easily understood when the probing wave propagates perpendicularly to the magnetic

surfaces and scattering angles are small (Fig. 1). From the beam spectrum $G(\kappa_\perp)$, we can readily obtain the instrumental selectivity function [9]

$$F(\boldsymbol{r}) = \exp[-(2k\sin(\xi(r)/2)/\Delta)^2] \,, \qquad\qquad (4)$$

where $\xi(r)$ is the change in pitch angles of magnetic field lines starting from the point where scattered waves are detected with maximum efficiency, i.e., from the aiming point of the receiving antenna.

From Eq. (4), we obtain the spatial resolution $\delta l \approx 2\Delta/k\langle d\xi/dr\rangle$, where $\langle d\xi/dr\rangle$ is the average derivative of the magnetic pitch angle inside the scattering region. Compared to the above estimate, Eq. (4) does not depend on the wave number of the probing wave. This is very advantageous for scattering of far infrared waves, since Eq. (4) gives a spatial resolution that is substantially smaller than the dimension of the common region between the probing and scattered beams. Unfortunately, very often this is not satisfactory because of the small value of $d\xi/dr$ in tokamaks, as in the case of the magnetic configuration of Fig. 2 with the magnetic pitch angle distribution of Fig. 3. In this case, we get the instrumental selectivity function of Fig. 4 for fluctuations with a wave number of 2 cm^{-1} and a probing beam (w=3) propagating on the tokamak mid-plane perpendicularly to the magnetic field. In spite of the fact that such a scattering geometry – indeed very impractical and difficult to implement – maximizes the benefits of magnetic shear, the instrumental selectivity function in Fig. 4 is very broad and would therefore result in poorly localized measurements.

In this paper, we will consider the general case of a probing beam propagating at an arbitrary angle with the magnetic field [14]. This is motivated by the fact that the conditions for coherent scattering become strongly dependent on the toroidal curvature of magnetic field lines when the probing beam forms a small angle with the magnetic field. This is schematically illustrated in Fig. 5, showing a case where the probing beam is on the tokamak mid-plane. For a given fluctuation wave number, the wave vector of the

<div align="center">5</div>

scattered wave (k_s) is parallel to the mid-plane only if the wave is scattered at one of the two points P_1 and P_2 (toroidally separated by an angle equal to the scattering angle), where the fluctuation wave vector (k) is in the plasma radial direction. At all the other probing locations, then, Eqs. (2) and (3) impose to the scattered wave to propagate at an oblique angle with the mid-plane. It is this phenomenon that we will exploit for localizing the scattering region. As we shall see in the following, its size depends on the spatial distribution of magnetic pitch angles and may become very small in standard tokamak plasmas [14]. Furthermore, we will find that this scattering scheme has the additional advantage of minimizing the radial resolution of fluctuation measurements, i.e., the footprint of the scattering region in the radial plasma direction.

3. Instrumental Selectivity Function

Throughout this paper, we will assess the localization properties of scattering measurements with an instrumental selectivity function - as defined by the collection efficiency of the receiving antenna - which was derived in Ref. [14]. For the sake of clarity and reader's convenience, here we summarize its derivation.

In the system of orthogonal coordinates (u,v,t) with the t-axis parallel to k_0, we define the polar angle φ with

$$k_{su} = k_0 \sin\theta\cos\varphi, \quad k_{sv} = k_0 \sin\theta\sin\varphi, \quad k_{st} = k_0 \cos\theta. \tag{5}$$

Let us now consider scattered waves originating from two points of the probing beam with identical scattering angles but different wave vectors k_s^1 and k_s^2, respectively (Fig. 6). From Eq. (5), we get

$$\frac{k_s^1 \cdot k_s^2}{k_0 \cdot k_0} \equiv \cos\alpha = \cos^2\theta + \sin^2\theta\cos\delta\varphi, \tag{6}$$

where $\delta\varphi = \varphi_2 - \varphi_1$, giving

$$\cos\alpha = 1 - \sin^2\theta(1 - \cos\delta\varphi) = 1 - 2\sin^2(\delta\varphi/2)\sin^2\theta. \tag{7}$$

6

For $\theta^2 \ll 1$ (always satisfied in this paper), this becomes

$$\alpha^2 \approx 4\theta^2 \sin^2(\delta\varphi/2). \qquad (8)$$

Suppose, then, that the launching and receiving antennae have similar electromagnetic properties, i.e., identical radiation patterns, with the latter positioned for collection with maximum efficiency of scattered waves from the first point. By replacing $\kappa_\perp$ with $k_0\alpha$ in the spectrum $G(\kappa_\perp)$, we obtain the collection efficiency of scattered waves from the second region

$$F = \exp\left(-\alpha^2/\alpha_0^2\right), \qquad (9)$$

where $\alpha_0 = \Delta/k_0$. This, together with Eq. (8) and the Bragg condition, gives the instrumental selectivity function

$$F = \exp[-(2k\sin(\delta\varphi/2)/\Delta)^2], \qquad (10)$$

where $k \approx k_0\theta$ is the wave number of detected fluctuations. In the case of a probing beam propagating perpendicularly to the magnetic surfaces, φ coincides with the magnetic pitch angle (apart from an additive constant) and Eq. (10) is equal to Eq. (4).

Finally, the polar angle φ can be obtained from Eq. (3), rewritten as

$$(\boldsymbol{k}_s - \boldsymbol{k}_0) \cdot \boldsymbol{B} = 0, \qquad (11)$$

from which we get

$$B_t(\cos\theta - 1) + B_u \sin\theta\cos\varphi + B_v \sin\theta\sin\varphi = 0, \qquad (12)$$

giving

$$\cos\varphi = \frac{B_u B_t(1 - \cos\theta) \pm \left[B_u^2 B_t^2(1 - \cos\theta)^2 - B_\perp^2\left(B_t^2(1 - \cos\theta)^2 - B_v^2 \sin^2\theta\right)\right]^{1/2}}{B_\perp^2 \sin\theta} \qquad (13)$$

and

$$\sin\varphi = \frac{B_t(1 - \cos\theta) - B_u \sin\theta\cos\varphi}{B_v \sin\theta}, \qquad (14)$$

where $B_\perp^2 = B_u^2 + B_v^2$, and with the ± sign corresponding to the two scattering branches of Fig. 5.

In the next section, these equations will be used for assessing the degree of localization of CO_2 laser scattering measurements in the next generation of burning plasma experiments. As test-bed we will use the tokamak configuration of Fig. 2 with the official ITER parameters [2]: plasma major radius=6.2 m, plasma minor radius=2 m, toroidal magnetic field on axis=5.3 T and plasma current=15 MA.

4. CO_2 Laser Scattering

We begin with the scattering geometry of Fig. 7, where a probing beam with a frequency of $3x10^{13}$ Hz and a waist (w) of 3 cm propagates on the tokamak equatorial plane along the x-axis, and the scattering receiver is set for the measurement of fluctuations with wave vectors parallel to the equatorial plane. Here and in the following we will use the system of orthogonal coordinates (x, y, z) of Fig. 7, and we will refer to the plane containing the magnetic axis as the equatorial plane, and to the (r-z) plane (with $r = \sqrt{x^2 + y^2}$) as the poloidal plane.

The beam ray trajectories, which in Fig. 7 are displayed on both equatorial and poloidal planes, are from a ray tracing code [15] including both wave refraction and first order diffraction effects. However, because of the large beam frequency, refractive effects are negligible. Furthermore, since $2x/k_0w^2 \ll 1$, diffraction effects are negligible as well, and consequently the beam radius remains nearly constant and equal to w.

Since $\theta \ll 1$, the two scattering branches of Fig. 5 have similar selectivity functions with maxima near the point ($x = 0$, $y = y_0$), where y_0 is the initial y-coordinate of the probing beam. For simplicity, we will consider only the scattering branch corresponding to the + sign in Eq. (13). We will also refer to the quantity $\varepsilon = (y_0 - r_{ma})/(y_b - r_{ma})$ (with y_b the maximum y-coordinate of the plasma boundary and r_{ma} the radius of the

8

magnetic axis) as the normalized radius of the scattering region, and we will consider only cases with positive values of ε, i.e., with the scattering region on the low-field side of the torus.

Figure 8 shows the instrumental selectivity function along the central ray of the probing beam for $\varepsilon = 0.5$ ($y_0 = 7.4$ m) and three values of k. As expected from Eq. (10), the width of F (defined as the distance δx of the two points where $F=1/e$) is a strongly decreasing function of k.

The corresponding components of $\boldsymbol{k}$ are displayed in Fig. 9, from which it appears that their relative amplitudes do not depend on the value of k. Indeed, this cannot be exactly true since $k_x = k^2/2k_0$ (Eq. (2)). However, since $k_x \approx 0$ because of the large k_0, the relative values of k_y and k_z are indeed insensitive to k. Finally, Eqs. (2) and (3) make k_z (equal to zero at the peak of F, near $x=0$) to grow towards the plasma boundary where, however, F is very small.

As shown in Ref. [14], the scattering region is located near the point where the angle between the probing wave vector and the magnetic field has its minimum value (β), with the width δx of F an increasing function of β. This can be easily understood by noting that near the magnetic axis, where the poloidal magnetic field is very small, $\beta = \theta/2$ (Fig. 5). In this case, then, the width of the instrumental selectivity function becomes $\delta x \approx 2r_{ma}\alpha_0 = 4r_{ma}/k_0 w$, which is much smaller than in Fig. 8 where $\beta = 14^{\text{o}} >> \theta$. On the other hand, we have already seen that the selectivity function becomes very broad for $\beta = \pi/2$ (Fig. 4).

The strong dependence of F on β is illustrated in Fig. 10, showing that the width of F is a growing function of ε. Because of the magnetic pitch angle profile of Fig. 3, β is also a growing function of ε (going from 4.3$^{\text{o}}$ for $\varepsilon = 0.15$, to 18$^{\text{o}}$ for $\varepsilon = 0.7$). Hence the conclusion that δx is an increasing function of β.

Another way of changing the value of β is by using a probing beam propagating at an oblique angle with the equatorial plane, as shown in Fig. 11 where the beam is again launched perpendicularly to the y-axis, but with an angle (γ) of $\pm 4.5^o$ with the x-axis (the $\pm$ sign indicating an upward and downward direction, respectively). To emphasize the role of β, here the launching points have been chosen to make the beam trajectory symmetric with respect to the equatorial plane. For $\varepsilon = 0.5$, this results in β varying from 9.5^o for $\gamma = -4.5^o$ to 18.5^o for $\gamma = +4.5^o$, with the corresponding value of δx increasing by more than a factor of two (Fig. 12) – again proving that the width of F is a growing function of β.

So far, we have considered the profile of the instrumental sensitivity function along the trajectory of the probing beam. Our results are summarized in Fig. 14, showing δx as a function of k for three radial positions. However, a crucial parameter of fluctuations measurements is their radial localization, which can be inferred from the distribution of F over the poloidal projection of the probing beam. More precisely, an estimate of the radial resolution can be obtained from the radial footprint (δr) of the set of points with $F > 1/e$, i.e., from $\delta r = \sqrt{(\delta x/2)^2 + y_0^2} - y_0$. This is displayed in Fig. 15, showing that δr becomes quickly much smaller than the beam diameter ($2w$) when $k > 2$ cm^{-1}. As noted above, because of a negligible wave refraction and diffraction, the beam radius is nearly constant and remains much smaller than any of the plasma scale lengths. Consequently, the results of Fig. 15 apply to all rays of the probing beam. Hence the conclusion that the radial resolution of scattering measurements is essentially determined by the diameter of the probing beam.

5. Wave Number Resolution

The instrumental selectivity function used so far was defined in Sec. 3 as the collection efficiency of waves scattered by fluctuations with the same value of k. In this

section, we generalize the definition of selectivity function to include fluctuations with all possible wave numbers. To be more precise, let us consider again scattered waves originating from two points of the probing beam with wave vectors k_s^1 and k_s^2, respectively. From Eq. (5), we get

$$\frac{k_s^1 \cdot k_s^2}{k_0 \cdot k_0} \equiv \cos\alpha = \cos\theta_1 \cos\theta_2 + \sin\theta_1 \sin\theta_2 (\cos\varphi_1 \cos\varphi_2 + \sin\varphi_1 \sin\varphi_2), \qquad (15)$$

where θ_1 and θ_2 are the corresponding scattering angles. From this, we obtain

$$\cos\alpha = \cos(\theta_2 - \theta_1) - 2\sin\theta_1 \sin\theta_2 \sin^2(\delta\varphi/2), \qquad (16)$$

where $\delta\varphi = \varphi_2 - \varphi_1$. Since both θ_1 and θ_2 are very small, this becomes

$$\alpha^2 \approx (\theta_2 - \theta_1)^2 + 4\theta_2\theta_1 \sin^2(\delta_\varphi/2). \qquad (17)$$

The mismatch angle between k_s^1 and k_s^2 is made of two terms. The first, as expected, is due to the difference in scattering angles. The second, as before, is due to the spatial variation of magnetic pitch angles.

Following the same procedure that led to Eq. (10), we obtain a new expression for the instrumental selectivity function

$$G = \exp\left[-\left((k'-k)^2 + 4k'k\sin^2(\delta_\varphi/2)\right)/\Delta^2\right], \qquad (18)$$

where $k \approx k_0\theta_1$ is the tuning wave number of the receiver, and $k' \approx k_0\theta_2$ is the wave number of detected fluctuations. For $k' = k$, we recover Eq. (10).

Contour plots of $G(k',x)$ are displayed in Fig. 16 for the same cases in Fig. 8. A comparison with the latter shows that the maximum width of G along the beam trajectory is similar to that of F. It also shows, as expected, that the wave number resolution remains $\approx \pm\Delta$.

Finally, the use of Gaussian beams – a crucial assumption in the scattering scheme of this paper – implies the availability of circular ports with substantially larger radii (r_w)

than w. Assuming the conservative criterion of $r_w \approx 2w$, the value of w used so far (3 cm) would require ports that are much smaller than the size of ITER. Hence we could envision using larger beams to obtain a substantial improvement in wave number resolution, as in Fig. 17 where the contour plots of $G(k',x)$ are displayed for w=6 cm.

6. Discussion

Throughout this paper, we have used an ITER-like plasma for deriving the properties of the proposed scattering scheme. However, since the instrumental sensitivity function depends only on the wave number of fluctuations, the radius and launching direction of the probing beam and the pitch angle of magnetic field lines, this scattering scheme will be capable of providing the same degree of spatial resolution in similar tokamaks. In other words, the ratio of δx to any of the plasma linear dimensions will be the same in tokamaks having identical aspect ratio, elongation, triangularity and magnetic safety factor. Indeed, since these quantities can vary only over a very narrow range of parameters, we may conclude that the advantages of the proposed scheme apply, mutatis mutandis, to any tokamak. This is demonstrated in Fig. 18, where the instrumental function for an IGNITOR-like plasma (major/minor radii=1.32/0.47 m, toroidal magnetic field=13 T, plasma current=12 MA [1]) is compared with that for ITER, showing an Iter/Ignitor ratio of 4.4 for δx, vis-à-vis one of 4.25 for the minor radii and 4.7 for the major radii (small discrepancy due to different aspect ratios, 3.1 vs. 2.8).

As stated in the Introduction, the benefits of CO_2 lasers stem from their high frequency and high power single-mode operation. However, since the instrumental selectivity function for a given value of k (Eqs. (10) and (18)) does not depend on the frequency of the probing beam, the use of lower frequencies would preserve the localization properties of scattering measurements. As a matter of fact, a scattering apparatus based on the scheme described in this paper and employing a backward wave

oscillator with a frequency of 2.8×10^{11} Hz is currently in use on NSTX for localized measurements of turbulent fluctuations driven by the ETG mode [16]. Obviously, the use of such a low probing frequency in a burning plasma experiment would defeat the spirit of this paper since both refractive and diffractive effects would become important. However, one could consider using other types of lasers, as for example those operating in the range of 3×10^{12} Hz (CH_3OH lasers).

Finally, it is worth noting that for the case of an ITER-like plasma the length of the scattering region along the probing beam (δx) will be much longer than in past CO_2 scattering measurements [4,7]. Consequently, since the power of scattered waves varies like δx^2, we conclude that the use of the proposed scheme in an ITER-like plasma will allow the detection of smaller fluctuation levels than in previous CO_2 scattering measurements.

7. Conclusion

In summary, the results presented in this paper illustrate how the short-scale turbulence that plasma theory indicates as a potential cause of anomalous transport in the next generation of burning plasma experiments could be detected with good spatial and wave number resolution using coherent scattering of CO_2 lasers.

The unique feature of the proposed scheme is the oblique propagation of the probing wave with respect to the magnetic field, with the toroidal curvature of field lines playing a major role in improving the spatial resolution of measured signals. Furthermore, this scattering geometry has the additional advantage of reducing the footprint of the scattering region in the plasma radial direction. Finally, small scattering angles and negligible wave refraction effects minimize the size of needed ports – a matter of vital importance for a plasma diagnostic that must operate in the hostile environment of a burning plasma.

Acknowledgement

REFERENCES

[1] B. Coppi, B. Nassi, and L. E. Sugiyama, Phys. Scr. **45**, 112 (1992).

[2] *Technical Basis for the ITER Final Design*, ITER EDA Documentation Series No. 24, IAEA, Vienna (2001).

[3] W. Horton, Rev. Mod. Phys. 71, 735 (1999).

[4] J. W. Connor and H. R. Wilson, Plasma Phys. Control. Fusion **36**, 719 (1994).

[5] E. Mazzucato, Phys. Rev. Lett.. **36**, 792 (1976).

[6] C. M. Surko and R. E. Slusher, Phys. Rev. Lett.. **37**, 1747 (1976).

[7] D. L. Brower, W. A. Peebles, and N. C. Luhmann, Jr., Nucl. Fusion **27**, 2055 (1987).

[8] R. Philipona, E. J. Doyle, N. C. Luhmann, Jr., W. A. Peebles, C. Rettig, K. H. Burrell, R. J. Groebner, H. Matsumoto, and the DIII-D Group, Rev. Sci. Instrum. **61**, 3007 (1990).

[9] P. Devynck, X. Garbet, C. Laviron, J. Payan, S. K. Saha, F. Gervais, P. Hennequin, A. Quéméneur, and A. Truc, Plasma Phys. Control. Fusion **35**, 63 (1993).

[10] R. Fonck, G. Cosby, R. D. Durst, S. F. Paul, N. Bretz, S. Scott, E. Synakowski, and G. Taylor, Phys. Rev. Lett.. **70**, 3736 (1993).

[11] E. Mazzucato and R. Nazikian, Phys. Rev. Lett. **71**, 1840 (1993).

[12] E. Mazzucato, Rev. Sci. Instrum. **69**, 2201 (1998).

[13] M. N. Rosenbluth and N. Rostoker, Phys. Fluids **5**, 776 (1962).

[14] E. Mazzucato, Phys. Plasmas **10**, 753 (2003).

[15] E. Mazzucato, Phys. Fluids B **1**, 1855 (1989).

[16] D. R. Smith, E. Mazzucato, T. Munsat, H. Park, D. Johnson, L. Lin, C. W. Domier, M. Johnson, and N. C. Luhman, Jr, Rev. Sci. Instrum. **75**, 3840 (2004).
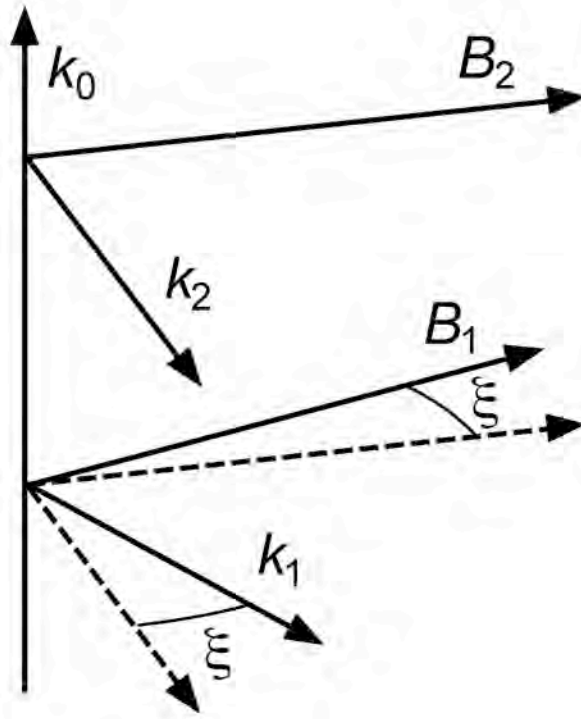
Figure 1. Magnetic field (B_1 and B_2) and fluctuation wave vector (k_1 and k_2) at two points of a probing beam (k_0) propagating perpendicularly to the magnetic surfaces. Scattering angles are equal (i.e., $k_1=k_2$) and small (i.e., k_1 and k_2 are nearly perpendicular to k_0).
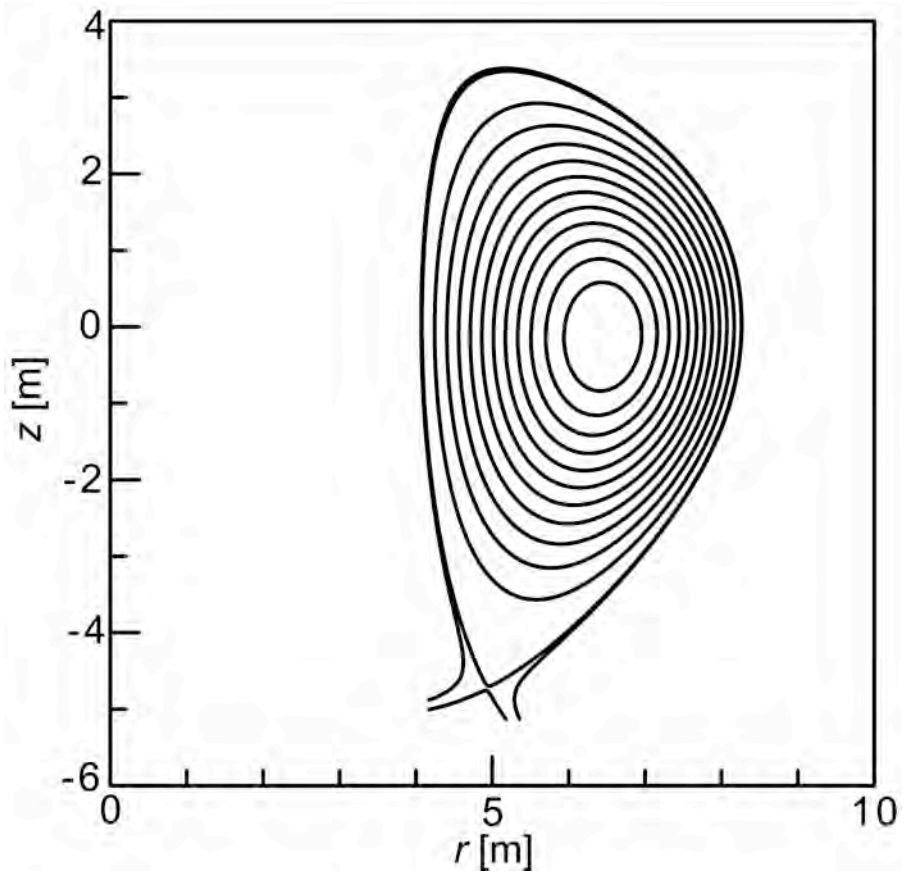
Figure 2. Poloidal cross section of an ITER-like tokamak used throughout the paper for deriving the properties of the proposed scattering scheme.
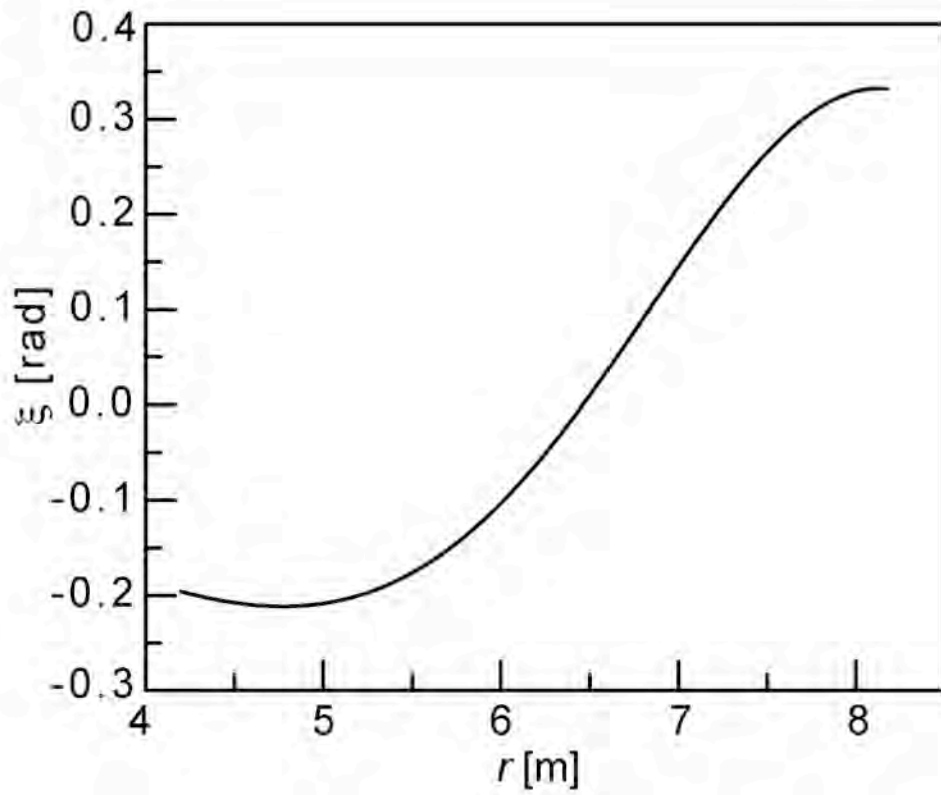
Figure 3. Pitch angle of magnetic field lines on the equatorial plane of the tokamak configuration of Fig. 2.
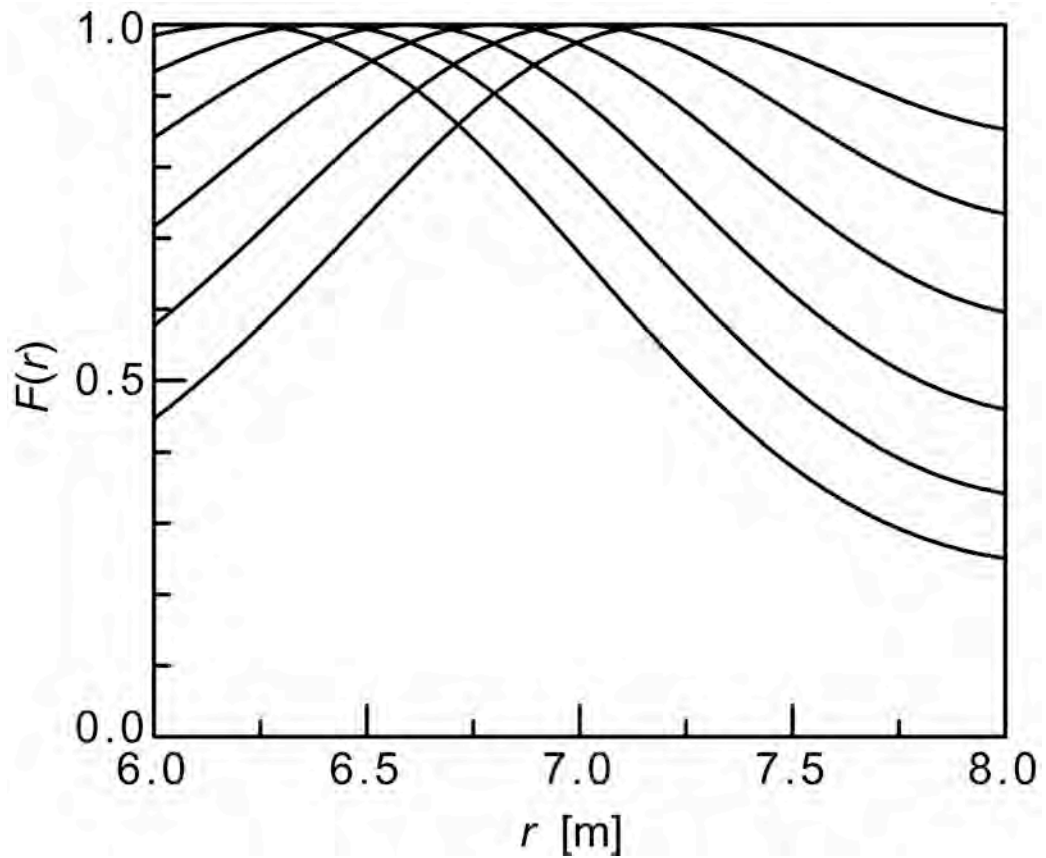
Figure 4. Instrumental selectivity functions for detection of fluctuations with $k=2$ cm^{-1} at several radial locations. The probing beam has a radius of 3 cm and propagates on the equatorial plane perpendicularly to the magnetic field.
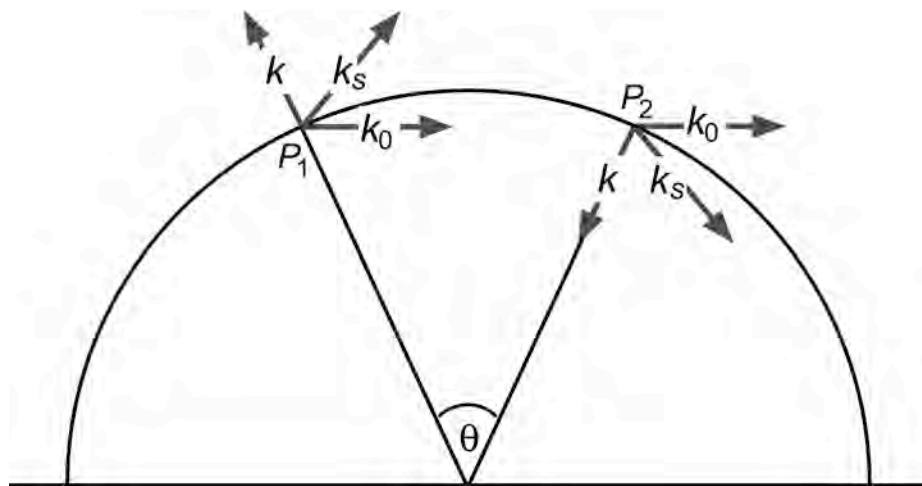
Figure 5. Scattering geometry with the probing beam (k_0) on the tokamak mid-plane. For a given fluctuation wave number (k), Eqs. (2) and (3) are satisfied only at P_1 and P_2 (toroidally separated by the scattering angle θ).
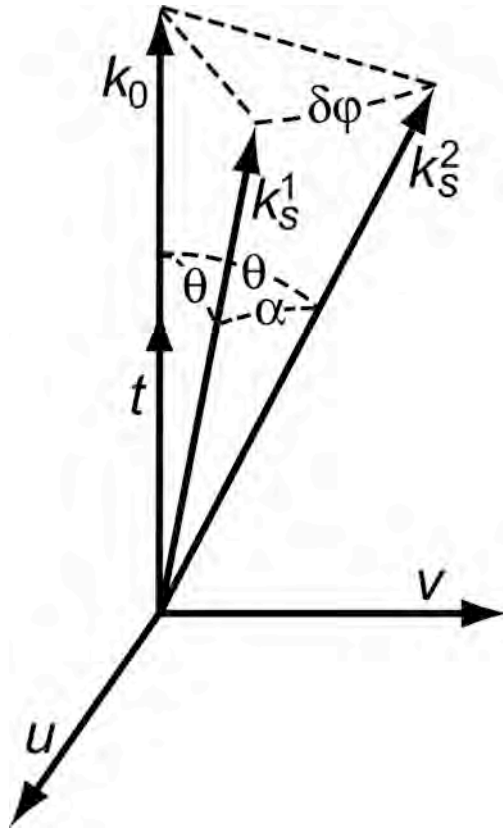
Figure 6. Orthogonal coordinates (u,v,t) with the t-axis along the wave vector of the probing beam ($\mathbf{k}_0$).
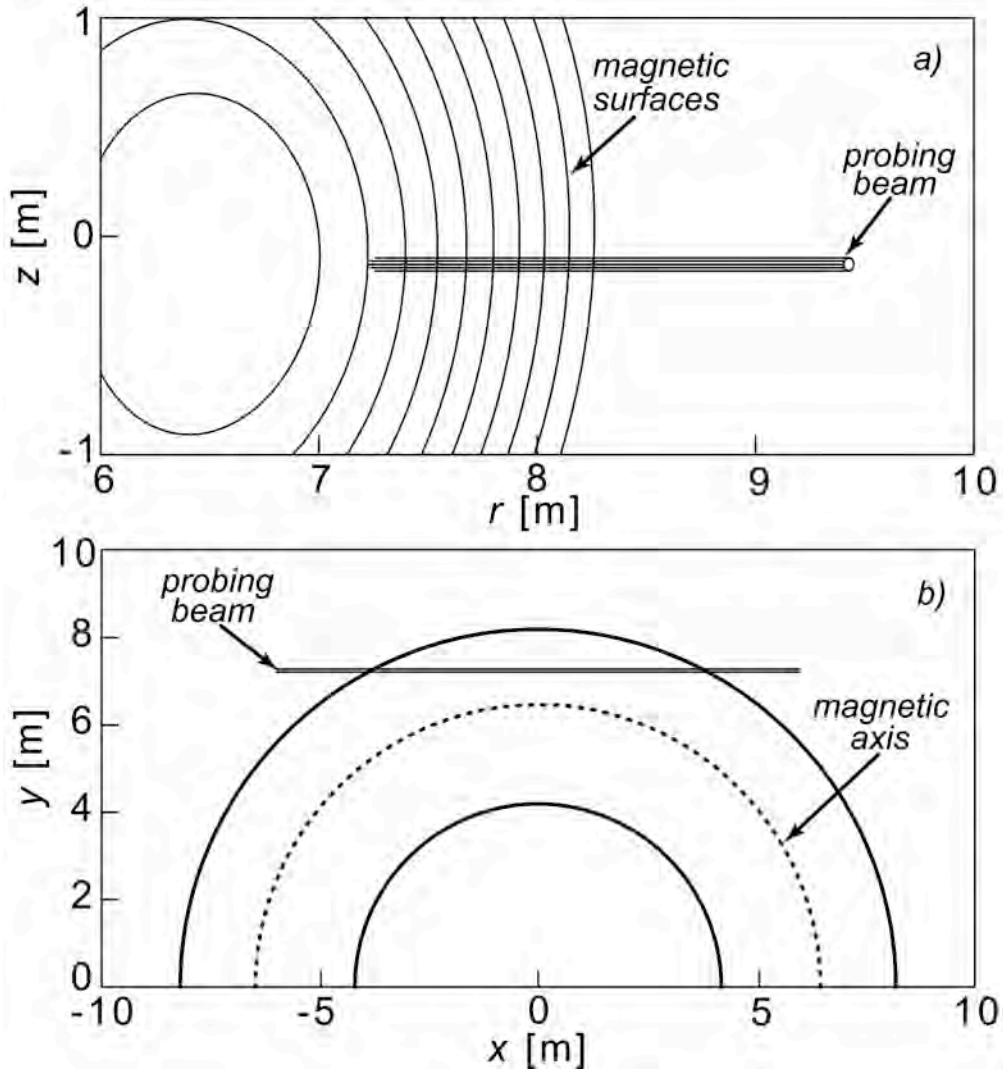
Figure 7. Poloidal (*a*) and toroidal (*b*) trajectories of a CO_2 Gaussian beam (*w*=3 cm) propagating on the equatorial plane of the tokamak of Fig. 2 with a peak plasma density of 1×10^{20} m^{-3}.
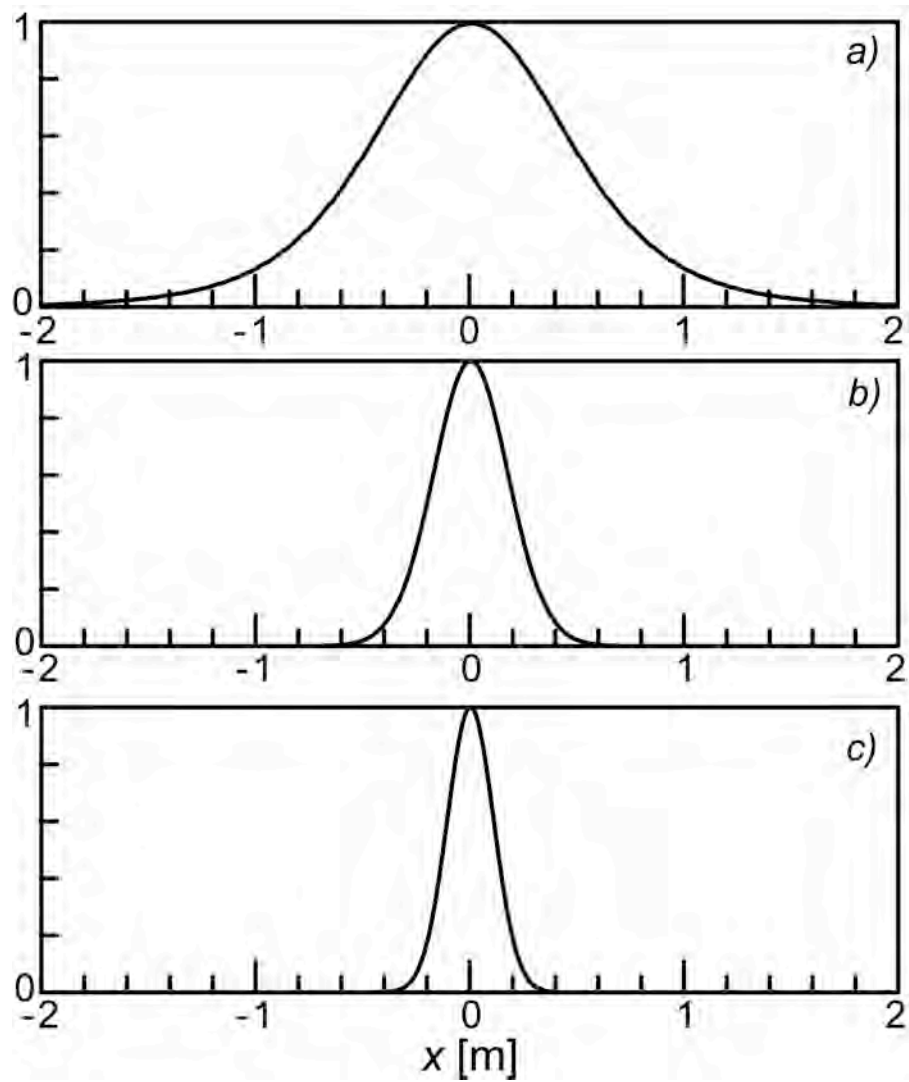
Figure 8. Instrumental selectivity function for the scattering geometry of Fig. 7 with $\varepsilon = 0.5$, $\beta = 14^\circ$ and (a) $k=2$ cm^{-1}, (b) $k=5$ cm^{-1}, (c) $k=8$ cm^{-1}.
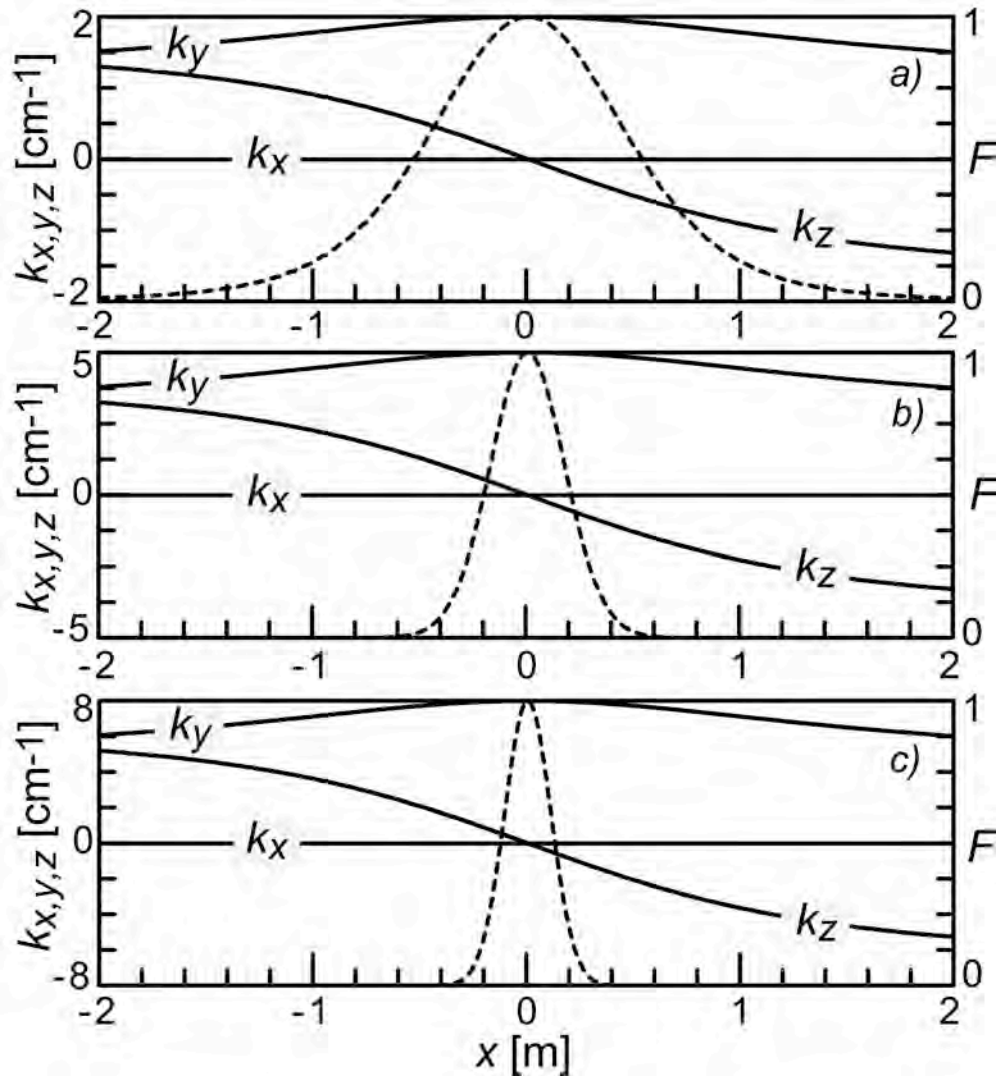
Figure 9. (*x, y, z*)-components of the wave vector *k* of detected fluctuations for the three cases in Fig. 8 (dashed lines are the instrumental selectivity functions).
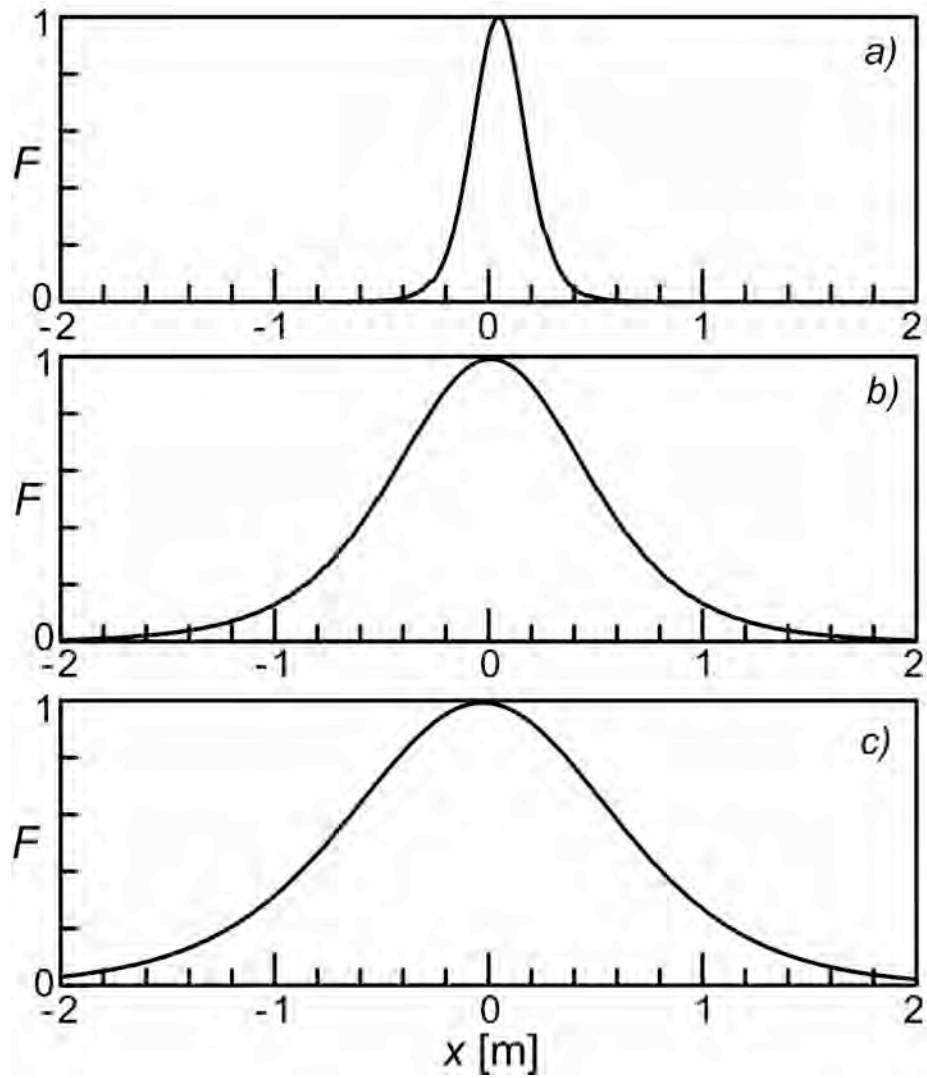
Figure 10. Instrumental function for the scattering geometry of Fig. 7 with $k=2$ cm^{-1} and (*a*) $\varepsilon = 0.15$ ($\beta = 4.3°$), (*b*) $\varepsilon = 0.5$ ($\beta = 14°$), (*c*) $\varepsilon = 0.7$ ($\beta = 18°$).
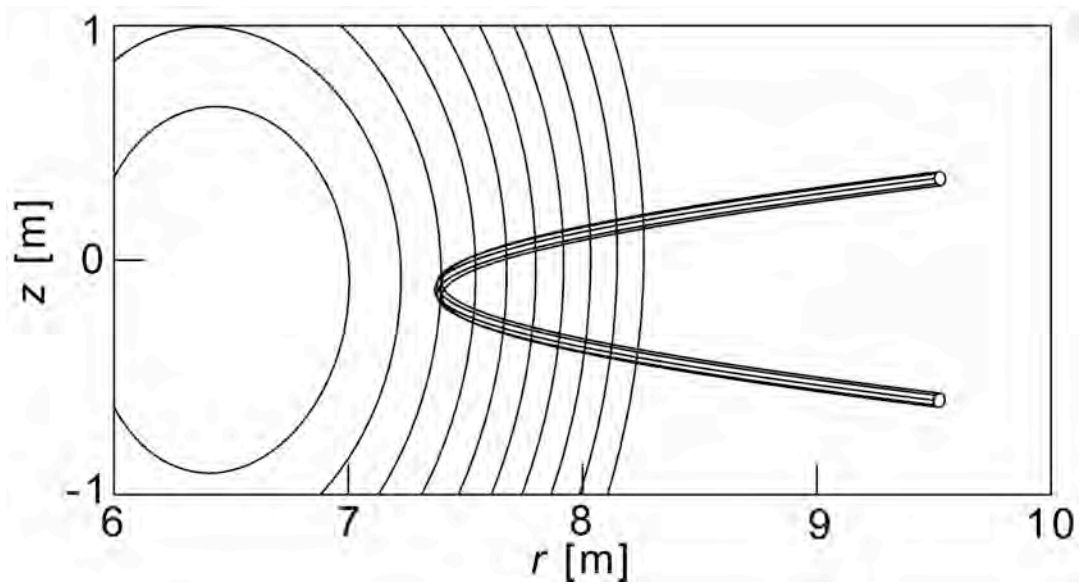
Figure 11. As in Fig. 7(*a*) with the probing beam making an angle of ±4.5º with the *x*-axis. Initial points are chosen to make the beam trajectory symmetric with respect to the equatorial plane.
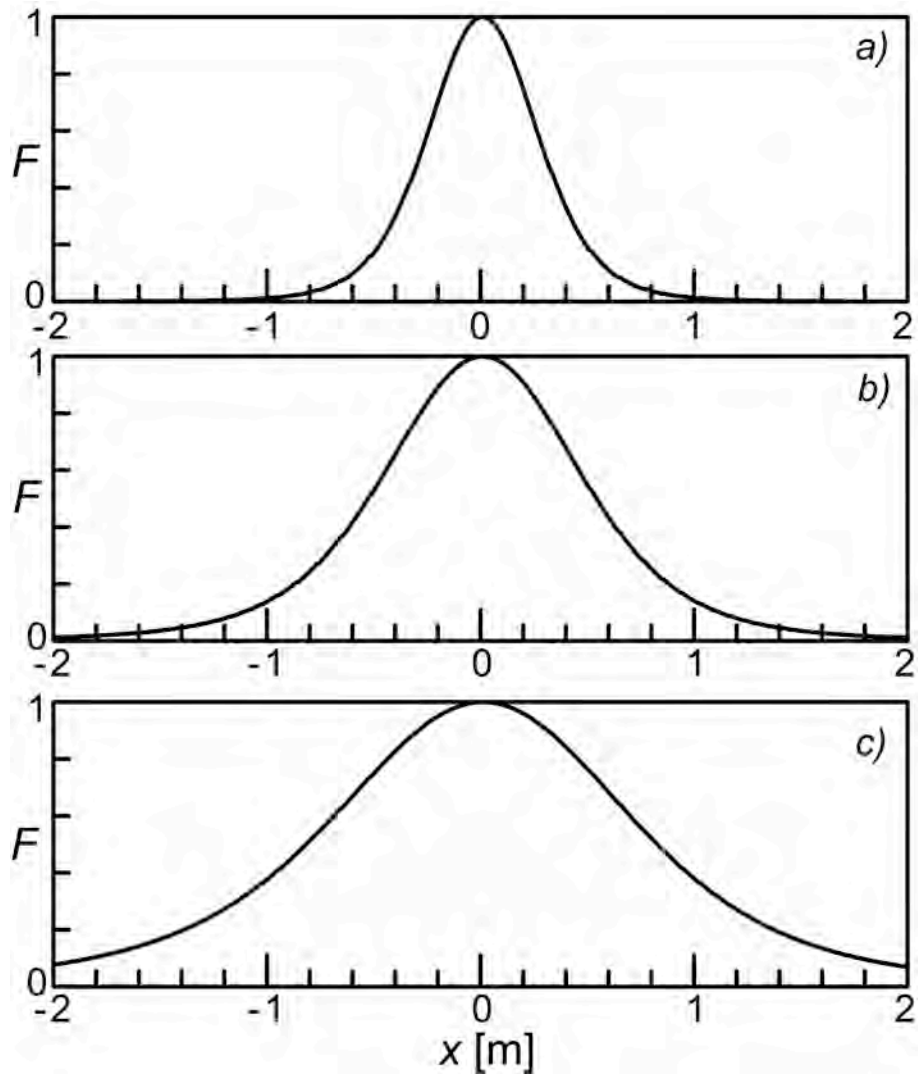
Figure 12. Instrumental function for $k=2$ cm^{-1}, $\varepsilon = 0.5$ and (*a*) $\gamma = -4.5^o$ ($\beta = 9.5^o$), (*b*) $\gamma = 0^o$ ($\beta = 14^o$), (*c*) $\gamma = +4.5^o$ ($\beta = 18.5^o$).
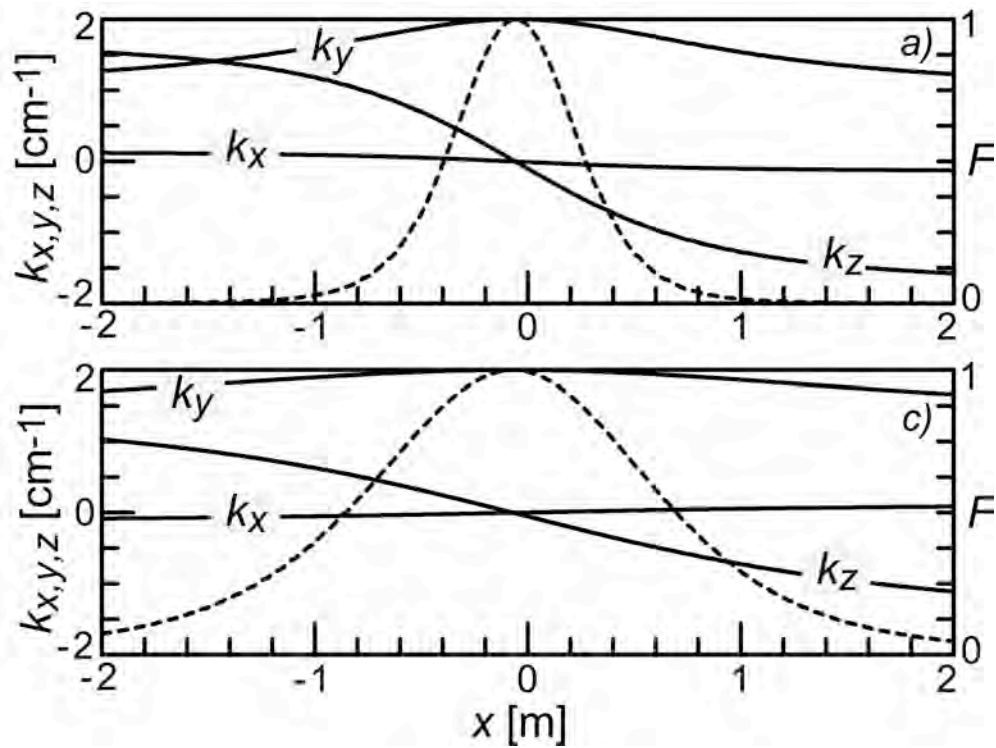
**Figure 13**. Same as in Fig. 9 for cases (*a*) [$\gamma = -4.5^o$, $\beta = 9.5^o$] and (*c*) [$\gamma = +4.5^o$, $\beta = 18.5^o$] of Fig. 12.
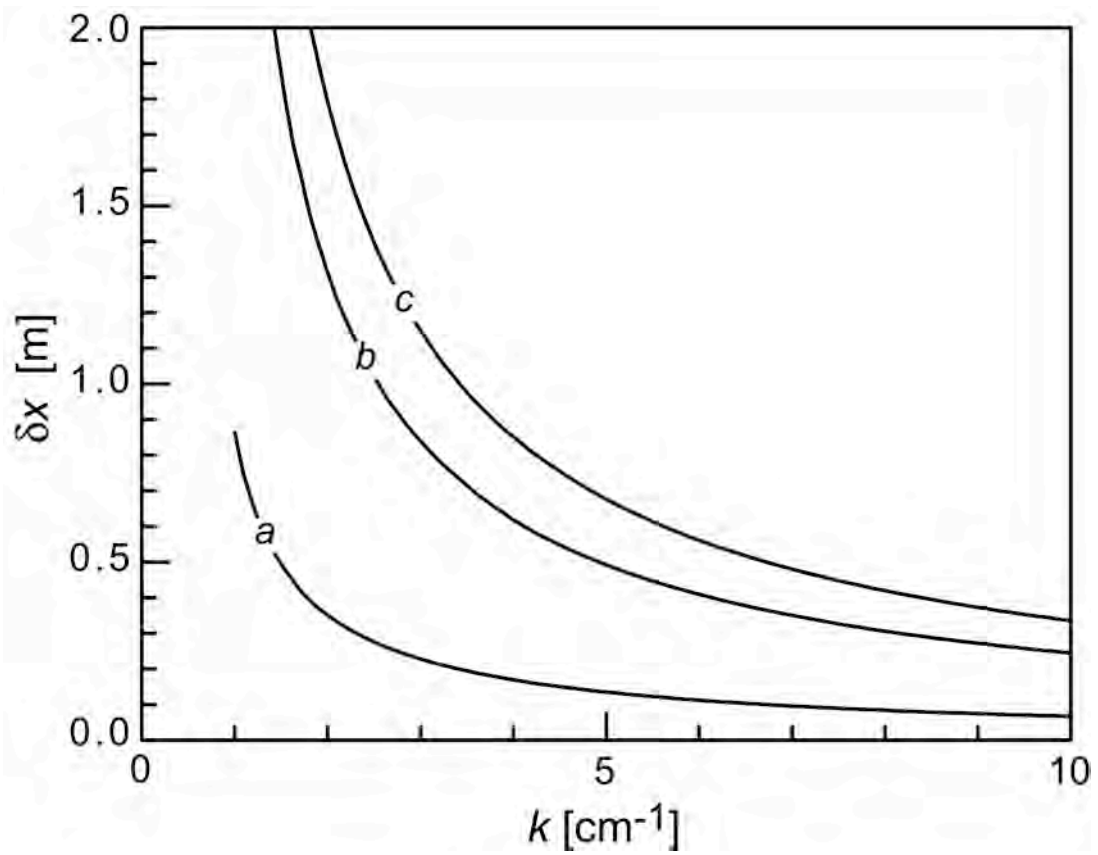
Figure 14. Width δx as a function of k along the central ray of a probing beam with $\gamma = 0^\circ$ and (*a*) $\varepsilon = 0.15$, (*b*) $\varepsilon = 0.50$, (*c*) $\varepsilon = 0.70$.
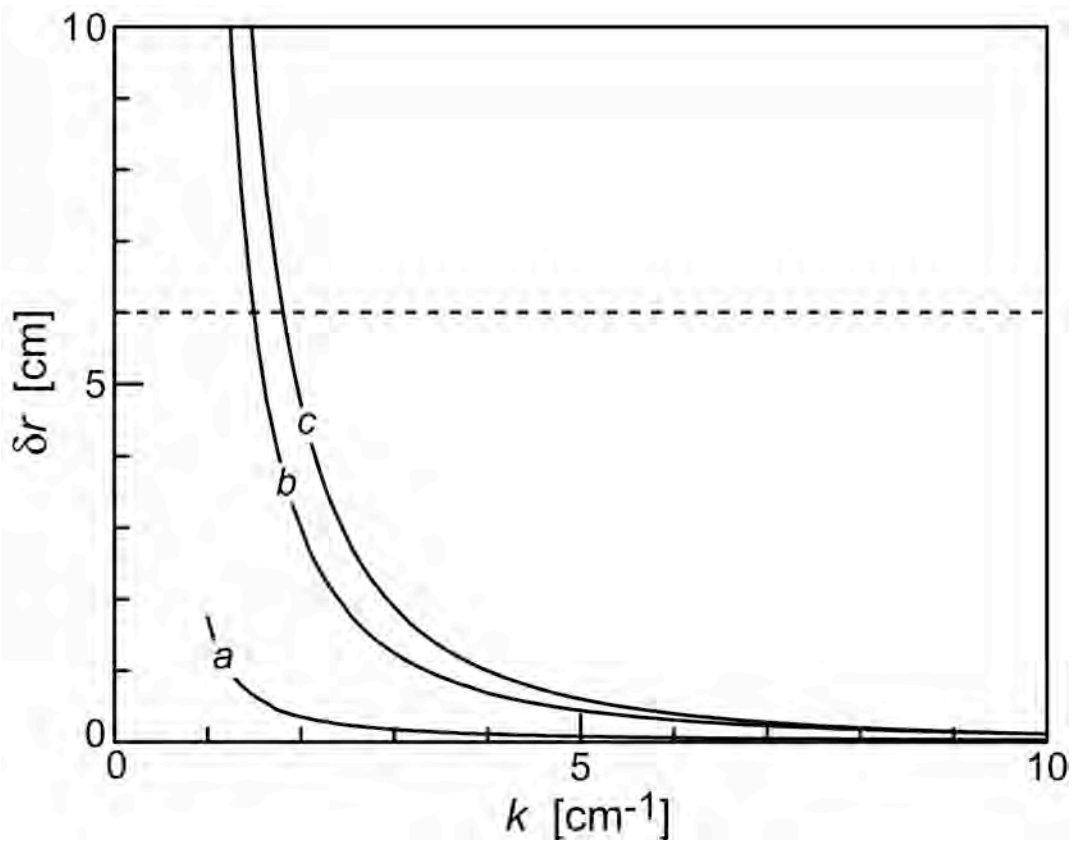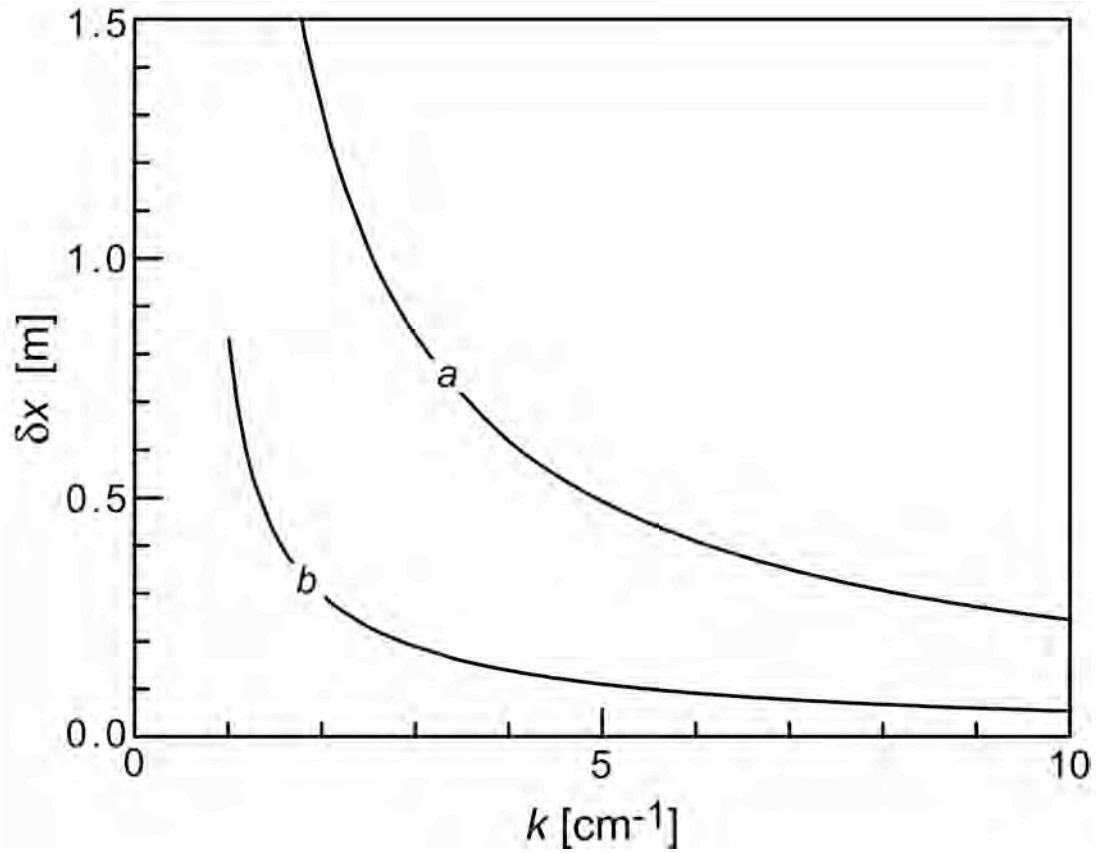
Figure 15. Radial footprint δr of the portion of central ray with $F > 1/e$ for the cases of Fig. 14. Dashed-line represents the beam diameter $(2w)$.
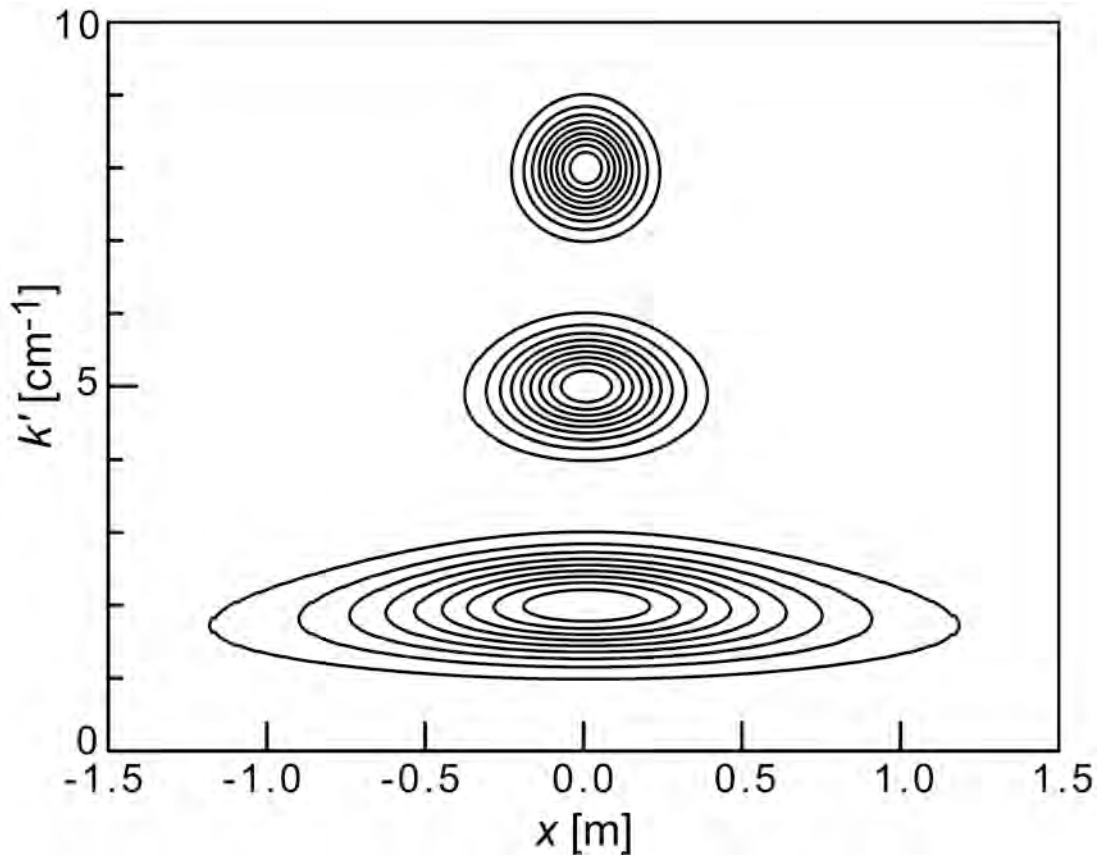
Figure 16. Contour plots (nine levels equally spaced from 0.1 to 0.9) of $G(k',x)$ for the three cases of Fig. 8.
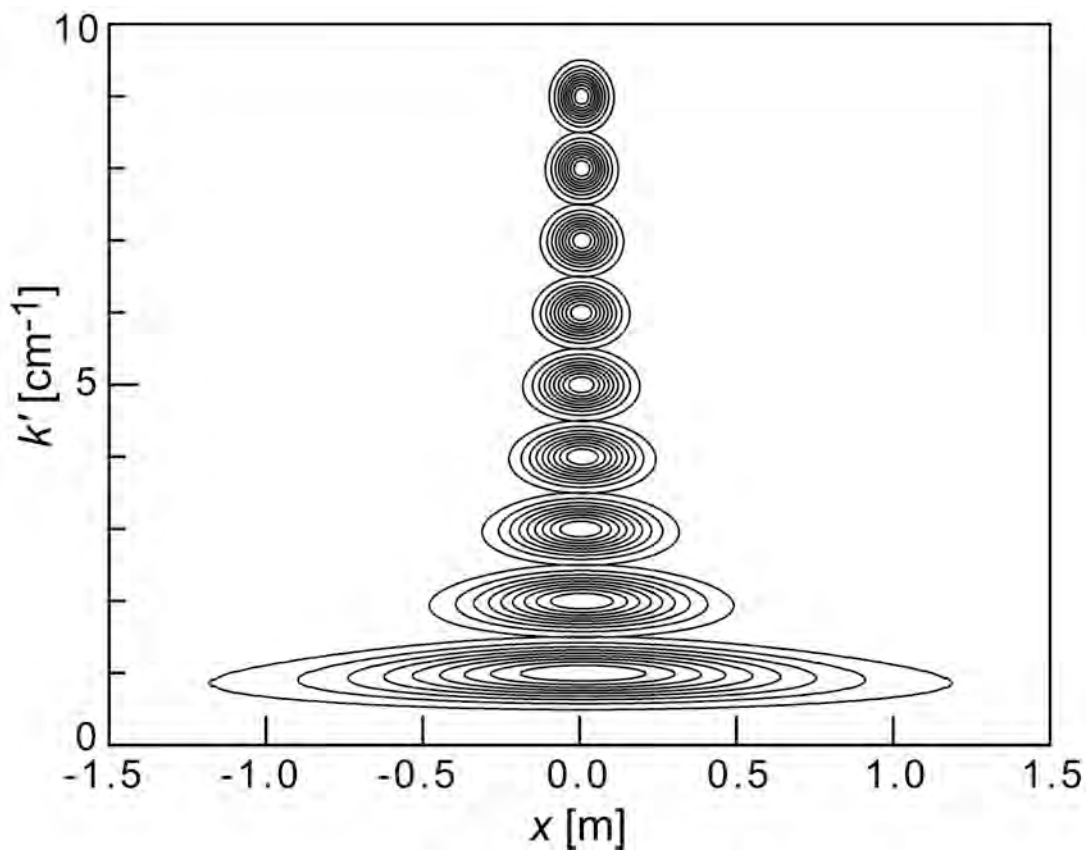
Figure 17. Contour plots (nine levels equally spaced from 0.1 to 0.9) of $G(k',x)$ for the scattering geometry of Fig. 7 with $\varepsilon=0.5$, $w=6$ cm and $k=1\text{-}9$ cm^{-1} (from bottom to top).

Figure 18. Width δx as a function of k for $\gamma = 0^o$ and $\varepsilon = 0.5$; (*a*) ITER, (*b*) IGNITOR.